HHS Public Access

Author manuscript

Analyst. Author manuscript; available in PMC 2021 September 28.

Published in final edited form as:

Analyst. 2020 September 28; 145(19): 6243–6253. doi:10.1039/d0an01373k.

Acoustofluidic Assembly of 3D Neurospheroids to Model Alzheimer's Disease

Hongwei Cai[a], **Zheng Ao**[a], **Liya Hu**[a], **Younghye Moon**[b], **Zhuhao Wu**[a], **Hui-Chen Lu**[c], **Jungsu Kim**[b], **Feng Guo**[a,*]

[a]Department of Intelligent Systems Engineering, Indiana University, Bloomington, Indiana 47405, United States

[b]Stark Neurosciences Research Institute, and Department of Medical and Molecular Genetics, Indiana University School of Medicine, Indianapolis, Indiana, 46202, United States

[c]Gill Center for Biomolecular Science, and Department of Psychological and Brain Sciences, Indiana University, Bloomington, Indiana 47405, United States

Abstract

Neuroinflammation plays a central role in the progression of many neurodegenerative diseases such as Alzheimer's disease, and challenges remain in modeling the complex pathological or physiological processes. Here, we report an acoustofluidic 3D culture system that can rapidly construct 3D neurospheroids and inflammatory microenvironments for modeling microglia-mediated neuroinflammation in Alzheimer's disease. By incorporating a unique contactless and label-free acoustic assembly, this cell culture platform can assemble dissociated embryonic mouse brain cells into hundreds of uniform 3D neurospheroids with controlled cell numbers, composition (e.g. neurons, astrocytes, and microglia), and environmental components (e.g. amyloid-β aggregates) in hydrogel within minutes. Moreover, this platform can maintain and monitor the interaction among neurons, astrocytes, microglia, and amyloid-β aggregates in real-time for several days to weeks, after the integration of a high-throughput, time-lapse cell imaging approach. We demonstrated that our engineered 3D neurospheroids can represent the amyloid-β neurotoxicity, which is one of the main pathological features of Alzheimer's disease. Using this method, we also investigated the microglia migratory behaviors and activation in the engineered 3D inflammatory microenvironment at a high throughput manner, which is not easy to achieve in 2D neuronal cultures or animal models. Along with the simple fabrication and setup, the acoustofluidic technology is compatible with conventional Petri dishes and well-plates, supports the fine-tuning of the cellular and environmental components of 3D neurospheroids, and enables the high-throughput cellular interaction investigation. We believe our technology may be widely used as in vitro brain models for modeling neurodegenerative diseases, discovering new drugs, and testing neurotoxicity.

Table of content

*Corresponding fengguo@iu.edu.

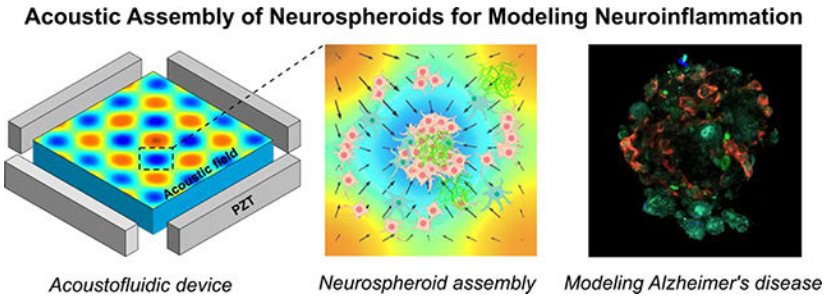

Keywords

Alzheimer’s disease; Neuroinflammation; Microglia; Acoustofluidics; Microfluidics; 3D Cultures

Introduction

Alzheimer’s disease (AD) is one of the most common neurodegenerative diseases, affecting an estimate of 50 million people worldwide.[1] Tremendous efforts have been made to study the pathogenesis of AD and establish clinical trials of various treatments. The amyloid-β plaques and neurofibrillary tangles have been generally considered as the key pathological hallmarks of AD. However, the etiology of AD is still largely unclear, and there is no effective clinical treatment despite high amounts of past and active research.[2] Recent advances in the microglia-mediated neuroinflammation research provide new insights into the cause of AD.[3] Microglia, a specialized population of macrophages-like cells in the central nervous system (CNS), are capable of orchestrating inflammatory responses in the CNS.[4–6] For example, it is known that microglia is involved in the synaptic organization, myelin turnover, control of neuronal excitability, phagocytic removal of cell debris or apoptotic cells, and protection of homeostatic brain.[7–10] In contrast, in the AD brain, it has been found that phenotypically activated microglia (or disease-associated microglia, DAM) is involved in the formation of the amyloid-β plaque. It was observed that microglia can recognize and response to amyloid-β peptide deposits, and migrate towards and interact with amyloid-β deposits. Moreover, there is increasing evidence to show that the pathogenic neuron and synapse loss were closely correlated with the aberrant activation of microglia. Thus, it is of great interest to study the microglia-mediated neuroinflammation in AD. Especially, the interaction of microglia within the complex brain microenvironment of AD (e.g. neurons, astrocytes and amyloid-β plaques) is still not well explored.[11, 12]

So far, the in vivo and 2D in vitro models have been intensively used for the understanding of the microglia-mediated neuroinflammation in AD. The in vivo animal models can recapitulate AD disease features by the transgenic expression of human familial AD genes which lead to spontaneously formation of Aβ plaques and neurofibrillary tangles.[13, 14] The animal models provide an ideal brain microenvironment for the study of microglia. However, animal models are largely inaccessible to real-time imaging and timely microglia manipulation.[15] Compared to the in vivo AD models, conventional 2D in vitro models are simple, convenient, and cost-effective for many different studies of microglia. For example, monolayer cultures of microglia have been widely used to study the basic functions of

microglia, such as migration and phagocytosis.[16] However, microglia cultured in such a 2D settings show dramatically different morphology and phenotype as compared with that in vivo. Microglia display a ramified morphology in 3D brain tissues, while the 2D cultured microglia tend to show an amoeboid morphology with an increased expression of proinflammatory and motility genes that are related to microglia activation.[17] Aside from the lack of 3D cell-cell contacts within the monolayer, the direct exposure of microglia to the serum-containing medium may contribute to the amoeboid morphology, which alters their gene expression profile as well as their phagocytosis ability.[18] Thus, there are tremendous needs to develop better in vitro microglial cultures for modeling neuroinflammation in AD.

To address the above issues of conventional 2D in vitro microglial cultures and better mimic the interaction of microglia with the complex brain microenvironment of AD, engineering efforts have been made by using microfluidics and/or biomaterials.[19–25] To understand microglial behavior at a single cell level, microfluidic channel and micropattern designs were used to study the migration of single microglia with controlled microenvironments (e.g., a gradient of amyloid-β peptides).[19, 20] For mimicking the interaction of microglia with other nerve cells, a microfluidic co-culture device integrated with micropatterned axons was developed to study the microglial phagocytosis of degenerating axons.[22] In addition, a neurovascular unit-on-a-chip system with multiple-layer microfluidic cultures was developed to study the microglial interaction with the neurons and astrocytes as well as their responses to neuroinflammation.[21] However, these microfluidic or engineered microglial cultures still cannot fully recapitulate the in vivo status of microglia such as their ramified morphology. To mimic the 3D brain tissue environment, biomaterial scaffolds were employed to support the 3D growth and culture of microglia. For example, 3D Matrix hydrogels were reported to support microglia to grow and maintain ramified morphology and enable the microglial response tests to proinflammation stimulus.[24, 25] Recently, by integrating the microfluidics and 3D Matrigel matrix, a tri-culture model was established to recapitulate the key features of AD neuroinflammatory processes.[23] This tri-culture system, consisting of human stem cell-derived neurons, astrocytes and microglia cultured within 3D Matrigel, was used to study the migration and phagocytosis of microglia as well as microglia-induced neurite degeneration and cell death in an AD brain-like environment. These engineered in vitro microglial culture approaches have brought significant advances versus the conventional 2D or monolayer microglial culture method. However, there is still an unmet need to better mimic the interaction of microglia with the complex brain microenvironment of AD. We believe that an ideal in vitro culture technology for modeling microglia-mediated neuroinflammation in AD should fulfill the following criteria: (1) rapid formation of the 3D physical contact among the microglia and other brain cells, (2) mimicking the microenvironment in AD brain tissues (e.g., a local gradient of oxygen and nutrients, avoiding or minimizing the serum exposure, and/or amyloid-β plaques), and (3) enabling high-throughput and multiple-condition testing.

As an alternative solution, acoustofluidics[26–30] may generate better 3D *in vitro* cultures to fill most of the above criteria for modeling AD neuroinflammation and studying microglia functions. This technique combines acoustic waves with microfluidic or microfabricated devices for the manipulation and culture of cells. So far, several designs and strategies of acoustofluidics have been developed for the generation of 3D tumor spheroids and 3D

myoblast cultures. Bulk acoustic wave (BAW)-based devices were fabricated to aggregate cancer cells and myoblasts into cell clusters within microfabricated well devices or Petri dishes, respectively.[31, 32] Acoustic streaming-based centrifugation devices were integrated into well-plates to centrifuge cells together for generation 3D cancer cultures.[33, 34] We developed a series of surface acoustic wave (SAW)-based devices to assemble 3D tumor spheroids within microfluidic chambers or disposable capillaries and devices.[35–38] This acoustofluidic technology has several unique advantages over other techniques. First of all, acoustofluidic devices can assemble randomly distributed cells into numbers of 3D cell aggregates within minutes in a contact-free and label-free manner.[28] Moreover, the acoustofluidics also manipulates cell-cell contacts while maintaining cells in their native culture medium or supporting Matrigel gel.[39] Furthermore, the acoustofluidic technology provides excellent biocompatibility, and has been demonstrated to pattern and grow nerve cells such as Schwann cells.[40] Thus, the acoustofluidics may have a great potential to address current issues of microglial cultures via the rapid manipulation of cell-cell contacts and their surrounding microenvironments.

Herein, to better model AD neuroinflammation in vitro, we present an acoustofluidic 3D culture system, combining high-throughput acoustofluidic assembly, 3D cell spheroids cultures, microenvironment manipulation, and time-lapse imaging into one experimental setup. Compared to other in vitro microglial culture models, our acoustofluidic 3D culture system possesses several unique advantages: The acoustic field enables the assembly of hundreds of uniform 3D neurospheroids within minutes in a petri dish, and this rapid cell aggregation not only facilitates the contacts of microglia to other surrounding cells but also minimize the microglia's non-specific activation by culture medium during the aggregation process. By precisely tuning the cell type and number, as well as Aβ aggregates, our platform can construct 3D neurospheroids and microenvironments for modeling microglia-mediated neuroinflammation in AD. The integrated microscope in the culture system enables real-time monitoring and tracking of the interaction between microglia, neuron, astrocytes and Aβ plaques. Employing this 3D culture system, the toxic effects of Aβ aggregates to neurospheroids were investigated, and the dynamic cumulation and coverage of microglia to Aβ aggregates were observed under real-time monitoring. The activation of microglia and the toxic effects of Aβ aggregates were further validated by using immunostaining and qRT-PCR. Based on the simplicity, reliability, and capability to be scale-up, we believe our platform may not only advance the understanding of neuroinflammatory diseases such as AD, and Parkinson's disease, but also facilitate the mechanistic study of autoimmune diseases such as multiple sclerosis, rheumatoid arthritis, and Crohn's disease.

Results and discussion

Working principle

The acoustofluidic 3D culture system consisted of a 35 mm petri dish and an acoustofluidic assembly device for generation of 3D neurospheroids, as well as an integrated microscope for real-time monitoring of microglia activities. The acoustofluidic assembly device was made of four piezoelectric transducers (PZTs) arranged as orthogonal pairs integrated into

laser-cut frames. The cell culture petri dish was inserted into the center of the acoustofluidic assembly device (Figure 1a). When acoustic waves were applied to cell suspensions, cells were aggregated into 3D spheroids to mimic the AD or healthy microenvironment in vivo, which enable the observation of the interaction between different cell types and inflammatory components (e.g., Aβ aggregates) The central area of the petri-dish, where the two sets standing acoustic waves interacted, contained typically 100 pressure nodes. Dissociated brain cells (e.g. neurons, astrocytes, and microglia) and Aβ aggregates were uniformly pushed into pressure nodes to form 100 clusters (Figure 1b). By controlling the components of the cell suspension in the petri-dish, the 3D neurospheroids were acoustically-assembled to mimic the healthy or AD brain microenvironment, respectively (Figure 1c). Using this platform, we observed the neurotoxicity of Aβ aggregates and the interaction between microglia and Aβ aggregates (accumulation, coverage, and activation), at the single-cell resolution, in real-time for extended periods. These observations demonstrated that our acoustofluidic 3D culture system enabled the formation of physiologically-relevant brain tissue-mimetic 3D structures.

Acoustic cell assembly

We tested the capability of our acoustofluidic method for culturing and maintaining uniform cell clusters. Mouse neuronal cells, Neuro 2A (N2A), were used to optimize the acoustic cell assembly of our device. N2A cells (2×10^6 /mL) were first introduced into the petri-dish and evenly distributed in the suspension before applying acoustic fields. Once applying RF signals at 1 MHz, two orthogonal sets of acoustic standing waves were generated. Acoustic standing waves propagated into the inner chamber, interacted with each other, and formed a periodically-distributed Gor'kov potential, which has a dot-array-like distribution, and each dot has a 3D cylinder-shaped Gor'kov potential distribution. Consequently, cells were pushed into the periodically-distributed Gor'kov potential and formed hundreds of 3D cell aggregates with the similar spatial distribution (Figure 2a, and Movie S1). These 3D cell clusters or neurospheroids were monitored every 24 hours using a fluorescence microscope. To further quantify the spatial distribution of acoustically- assembled 3D cell clusters, the images of acoustic cell patterning were analyzed and plotted along the X and Y-axis (Figure 2b, c). Corresponding to the brightness oscillated along the X and Y axis of defined periodicity, the 3D cell clusters were located periodically ($\lambda/2 = 750$ μm) along the X and Y axis. We found the size of 3D cell clusters was very uniform (163 ± 12.5 μm) after measuring about 100 clusters. The brightness curve changed sharply at the edge of the assembled clusters, indicating the capacity of generating uniform and well-defined clusters using the acoustofluidic patterning method. After a 5-day culture, the firm 3D N2A cell clusters were formed with uniformed size, while remaining in a dot-array-like pattern (Figure 2d, e). From the detailed view of each cluster, the 3D cell aggregates grow smooth surfaces and contained firm and complex cell-cell contact. A cell viability test was conducted on the biocompatibility of our method. The viability of N2A cells during the assembly and culture process showed no significant difference as compared to cells without acoustical assembly (Figure 2f). When the cell aggregates were formed and cultured in the Petri dish, high cell viability was maintained for 5 days (>90%). Thus, we demonstrated our method can generate intact and viable cell aggregates that are suitable to further model neuroinflammation.

Amyloid-β toxicity

Aβ plagues or aggregates are considered as one of the key contributors to AD and they are associated with neurotoxicity and neuron dysfunction.[41] To demonstrate the potential of acoustic methods for modeling AD, the neurotoxicity of Aβ aggregates were measured using acoustically assembled 3D neurospheroids. To explore how Aβ affects 3D neurospheroids, Aβ aggregates (5 μM) were acoustically-assembled with dissociated primary neuronal cells from an in vivo embryonic mouse brain to form cell clusters or neurospheroids with Aβ aggregates (Aβ+). The same primary neural cell suspension was also acoustically-assembled without Aβ aggregates as control groups (Aβ-). These engineered 3D neurospheroids were imaged and measured every day from day 0 (after acoustic assembly) until day 5 (Figure 3a). At day 0, the average size of Aβ+ and Aβ− 3D neurospheroids was similar, showing that the two groups had similar primary neuron numbers at the starting point (Figure 3b). During the first two days after acoustic assembly, the size of 3D neurospheroids in both groups showed an initial decrease since cells start to aggregate and form cell-cell contacts. Following initial spheroid formation, the size of Aβ− 3D neurospheroids remained unchanged in the following three days. In contrast, the spheroid size of Aβ+ 3D neurospheroids significantly decreased over the following three days. The average size of Aβ+ neurospheroids (82.1 ± 16.3 μm) was much smaller than that of Aβ− neurospheroids (121.3 ± 21.7 μm) indicating the neurotoxic effects of Aβ aggregates as the neuron death in the presence of Aβ aggregates. Thus, our 3D models demonstrated that neurotoxic effects of Aβ aggregates, which is consistent with previous reports that Aβ aggregates contribute to the neuron death in AD brain.[42]

Model Alzheimer's disease

Other than the neurotoxicity of Aβ aggregates, the AD brain contains more complex pathology, which is highly related to neuroinflammation.[23, 43] The key identities associated with AD are neurons, microglia, and Aβ aggregates. To provide a more physiologically relevant system to mimic key pathological features in AD, we acoustically-assembled neurons, Aβ aggregates, and microglia together into 3D neurospheroids (Figure 4a). Our platform can assemble randomly-distributed cellular and environmental components into uniform 3D neurospheroids in a Petri dish, enabling a realistic model to study the complex interactions among these components. The fluorescently-labeled BV-2 microglia (Red), Aβ aggregates (Green), and primary neurons (Blue) were acoustically assembled in the trapping nodes and formed clusters (Figure 4b). To better mimic the in vivo conditions, we tuned the ratio of microglial cells to primary neurons inside our neurospheroids by tuning the ratio of cell suspension and finally set to be a similar ratio as in an in vivo brain (1:10).[44] As our confocal images showed, the inner components of the 3D neurospheroids, the microglia (Red), Aβ aggregates (Green), and primary neurons (Blue) were uniformly located in the 3D neurospheroids (Figure 4c). These observations demonstrated that our acoustofluidic device enabled the formation of physiologically relevant 3D Aβ+ neurospheroids with the key cell types and inflammatory components.

Accumulation of microglia surrounding amyloid-β aggregates

In the early stage of AD, microglia migrate to Aβ plagues,[45, 46] forming a protective barrier to protect brain tissue from the neurotoxicity of Aβ plaques, and promotes the clearance of Aβ aggregates.[47, 48] As microglia and Aβ aggregates distributed uniformly in the acoustically assembled 3D neurospheroids, our AD model provided a realistic model for studying the accumulation of microglia around Aβ aggregates. The acoustically-assembled 3D neurospheroids were monitored using a confocal fluorescence microscope every day. The confocal images of stacks of 3D Aβ+ neurospheroids with labeled microglia (Red) and Aβ aggregates (Green) were analyzed to reveal the accumulation of microglia to Aβ aggregates. On day 0, nearly no microglia were located around the Aβ aggregate, as time went by, more microglia accumulated around the Aβ aggregates (Figure 5a). We further quantified the microglia accumulation to Aβ aggregates by quantifying the numbers of microglia near the Aβ aggregates (< 20 μm distance). The numbers of nearby microglia increased in the first two days up to 3 microglia per aggregate and stabilized after two days (Figure 5b). The microglia in the 3D Aβ+ neurospheroids accumulated to the surrounding of Aβ aggregates and the results were consistent with the previous findings in human AD brains and mouse models,[45, 48] indicating our model provided a realistic platform to monitor the microglia accumulation in real-time.

Coverage of microglia to amyloid-β aggregates

The microglia in the AD brain tightly cluster and cover around Aβ plagues and protect surrounding tissues from neurotoxicity and Aβ deposits.[49, 50] Thus, we further analyzed the coverage of microglia to Aβ aggregates. After a 5-day culture, microglial cells accumulated to the Aβ aggregates, and clustered tightly surround those aggregates. We found that the coverage of microglial cells to small (< 10 μm, Figure 6a), medium (10 ~ 20 μm, Figure 6b), and large (> 20 μm, Figure 6c) sized aggregates varied. With about 100 microglia and amyloid-β aggregates from 5 batches of neurospheroids, we quantified the extent to which the surface of individual Aβ aggregates was covered by the adjacent microglia in the acoustic assembled clusters using ImageJ. Larger aggregates (49.3%) tended to have less microglia coverage than the smaller ones (83.2%) (Figure 6d). In this study, we did not observe the ramified microglial cells. This may stem from the BV-2 cells, a transformed microglia cell line with differed morphology compared to microglia directly isolated from the animals,[48] which was reported previously.[51–53] The observed relation of coverage and aggregate size was consistent with the previous in vivo study,[48] indicating our 3D neurospheroids can recapitulate the behavior of microglia in vivo.

Microglia activation

In AD, brain microglial cells are activated in response to Aβ and other neuropathological changes and undergo complex neuroinflammation processes,[54] playing either a protective or detrimental role in the disease.[55, 56] To check the activation status of microglia in our cell culture system, 3D neurospheroids in the absence or presence of Aβ were analyzed via both immunostaining and quantitative reverse transcriptase-polymerase chain reaction (qRT-PCR). After a 5-day culture, the 3D neurospheroids with or without Aβ aggregates were immune-stained following cryo-sectioning. The 3D neurospheroids with the presence of Aβ

aggregates (Thioflavin-T) expressed a higher level of ionized calcium-binding adaptor molecule 1 (Iba-1, microglia marker) and lower level of microtubule-associated protein 2 (MAP-2, neuron marker) than those without Aβ aggregates (Figure 7a, b), indicating the Aβ aggregates activated the microglia and may induce the neurotoxicity as shown in Figure 3 b. The qRT-PCR results of neuron marker NeuN and microglia marker Iba-1 also showed the same corresponding to the immunostaining results (Figure 7c). The Iba-1 expression in our 3D Aβ+ neurospheroids was about 7 folds higher than that in the 3D Aβ− neurospheroids. The upregulated expression of Iba-1, indicating activation of microglia, were consistent with the previous finding in vivo.[57, 58] Taken together, our engineered 3D neurospheroids modeled the neuroinflammation such as the activation of microglia, which may provide a realistic 3D in vitro model for AD study.

Conclusions

In summary, we developed a novel acoustofluidic 3D culture system for modeling AD. The rapid acoustofluidic assembly of cells enables the generation of hundreds of 3D neurospheroids with uniformly distributed cell identities and environmental components in minutes. The 3D neurospheroids recapitulate important cell-cell contacts and suitable microenvironment for maintaining microglia function instantly after acoustic assembly. This method was used to investigate the neurotoxic effects of Aβ, demonstrating decreased cell viability and increased neurotoxicity, which are the key pathophysiological features of AD in vivo. Moreover, this platform was employed to study the coverage of Aβ aggregates by microglia, demonstrating the migration of microglia to Aβ aggregates, as observed an in vivo brain. Our acoustofluidic 3D culture system established the in vivo-like brain microenvironment. Therefore, it could fill the gap between traditional in vitro neuronal cell culture models and in vivo brain studies, serving as a more reliable tool for studying neurologic disease pathology and treatment strategies as well as drug screening applications.

Experiments

Device design and fabrication

The acoustic assembly device consists of four PZTs (PZT-41, Yuhai Electronics Ceramics, Co. Ltd, China) embedded into a laser-cut substrate and a cell culture dish. A 9 mm thick acrylic sheet was laser cut into the substrate of the device with an inner chamber of 40mm x 40mm and four small outer chambers for four embedded PZTs. The PZTs (dimension, 20 mm x 10 mm x 3mm; resonant frequency, 1MHz) were affixed to the outer chambers with epoxy, and a 3 mm thick acrylic sheet was glued to the substrate bottom to allow the chamber to contain DI water. The opposite two PZTs were wired together to a pair, and two pairs of PZTs were driven independently by two unsynchronized 1 MHz RF signals. The RF signals were generated by a function generator (TGP3152, Aim TTi) and amplified by a power amplifier (LZY-22+, Minicircuit) to drive the acoustic assembly device. A cell culture dish (35mm, Greiner Bio) was employed to contain cell suspensions and avoid contamination during the acoustic assembly process, the water-filled acrylic cavity was used to guide acoustic wave into the petri dish.

Numerical Simulation

The numerical simulation of acoustic Gor'kov potential field was conducted using COMSOL Multiphysics 5.2a. Figure S1b shows the simulation domain of the problem. To reduce computational amount, we only considered the fluidic domain (water). The four PZTs were considered as plane incident waves boundary conditions at the four sides of the fluidic domain. The upper and bottom sides of the fluidic domain were set to be plane wave radiation boundary condition. A "Frequency Domain" solver was used to calculate the problem. Figure S1c shows the three-dimensional distribution of the acoustic Gor'kov potential field. The pressure nodes and pressure anti-nodes are in cylinder like shape and locate in rectangular array.

Experiment operation

In the acoustic assembly experiment, cell suspension (2×10^6 /mL) in phosphate-buffered saline (PBS) supplied with 5% Gel-MA (Sigma-Aldrich) and 1% Irgacure D-2959 (Sigma-Aldrich) were introduced into the acoustic pattern chamber. RF signals (1MHz, 10 to 25 Vpp) were applied to the PZTs to generate acoustic trapping patterns. After a 2-minute acoustic patterning, the solution was crosslinked for 30 seconds using ultraviolet light (365 nm, 6 m W/m^2). The crosslinked solution containing 3D neurospheroids was transferred to a glass-bottom 24-well plate (MatTek Corporation) for confocal imaging and cultured in the corresponding culture medium.

Cell culture

Neuro 2A (N2A) cells were cultured in Dulbecco's Modified Eagle's Medium (Corning, NY) supplemented with 10% fetal bovine serum (Sigma Aldrich, MO), 2mM GlutaMAX-1 (Gibco), 100 U/mL penicillin and 100 μg/mL streptomycin (Invitrogen, PA). BV-2 microglial cells were cultured in Dulbecco's Modified Eagle's Medium (Corning, NY) supplemented with 2% fetal bovine serum (Sigma Aldrich, MO), 100 U/mL penicillin and 100 μg/mL streptomycin (Invitrogen, PA). All the cells were maintained in a humidified incubator at 5 % CO_2 and 37 °C.

Primary neuron culture

Primary neurons were isolated from cerebral regions of untimed (around E18) embryonic CD1 fetal mice (Envigo) using a surgical procedure approved by the Institutional Animal Care and Use Committee (IACUC) of Indiana University Bloomington. Cerebral regions were dissociated into cell suspension using the Papain dissociation system (Worthington Biochemical Corporation) following the manufacture's instruction. Primary neurons were maintained in Neurobasal medium containing B27 supplement [1 ml/ 50 ml], 0.5 Mm Glutamine Solution, 25 μM Glutamate (MW 147.13 g/Mol), and 1% antibiotic solution containing 10 000 units penicillin (Gibco) and streptomycin.

Amyloid-β aggregates preparation

Synthetic Aβ (BioLegend) was dissolved to 1mM in 100% HFIP, aliquoted and evaporated in Nitrogen gas. The aliquots were stored at −80 °C before use. For Aβ aggregates

preparation, the peptide is first resuspended in dry DMSO to 5 mM. PBS was added to bring the peptide to a final concentration of 100 μM, and shake the solution for 24 hours at 37 °C.

Cell viability assay

The live/dead staining was conducted using a LIVE/DEAD™ kit (Invitrogen) following the manufacture's instruction. For each test, about 100 neurospheroids were dissociated into single cells using Trypsin-EDTA. Then, these single cells were stained in medium supplemented with 2 μM of Carboxyfluorescein succinimidyl ester (CFSE) and 4 μM of ethidium homodimer (EthD) for 4 hours. And the cells were washed twice and replaced with a fresh medium, and then transferred to a well of 24 well plate for final measurement. Five views were randomly chosen under 4× microscope (3.2 mm × 3.2 mm), and over 500 cells were counted under each view. The staining results were visualized by an inverted fluorescence microscope (IX81, Olympus). Final cell viability was analyzed using ImageJ to account for the area of live/dead cells.

The label of amyloid-β and microglia

The prepared Aβ aggregates were stained with anti- Amyloid β (1:200, 6E10, Alexa 488, Biolegend) for 30 minutes before our acoustic assembly experiment. The BV-2 microglial cells were incubated in the serum-free culture medium supplied with red CMTPX dye (1:1000, CellTracker™, Invitrogen) for 30 minutes. The labeled BV-2 microglial cells were washed with fresh culture medium for 3 times before our acoustic assembly experiment.

Immunofluorescent staining

After 5 days of culture, the 3D neurospheroids were analyzed for neuronal and neural progenitor markers using immunostaining following cryo-sectioning. Brain organoids were washed three times with phosphate-buffered saline buffer (PBS) and fixed in 4% paraformaldehyde (in PBS) at 4°C overnight. Fixed organoids were then cryoprotected in 30% sucrose overnight at 4°C. Cryoprotected organoids were embedded in cryomolds (Sakura Finetek) with O.C.T compound (Fisher Healthcare) on dry ice. Embedded neurospheroids were sectioned on a cryostat to 20μm thickness slices. Spheroid slices were then incubated with corresponding primary antibodies at 4°C overnight. Respectively, slices were stained with anti-GFAP (1:500, BioLegend), anti-Iba1 (1:200, Biolegend) and anti-MAP2 (1:500, Millipore). After primary antibody incubation, corresponding secondary antibodies (Invitrogen, 1:500) were introduced, followed by Thioflavin-T staining. The neurospheroid slices were incubated in a solution of 0.5% of thioflavin T in 0.1 N HCl for 15 minutes. The staining results were viewed using a fluorescent confocal microscope (SP8, Leica).

Quantitative real-time PCR (qRT-PCR)

Neurospheroids were collected and lysed using RNeasy plus mini kit (Qiagen). The extracted RNA was then reverse-transcribed into complementary DNA (cDNA) using the qScript cDNA Synthesis Kit (Quantabio). Then gene expression of NeuN and IBA1 was then analysed by SYBR green-based qRT-PCR (Life technologies). The primer sequences were: NeuN forward: 5'-CCACTGAGGGAGACAAGAATA-3', NeuN reverse: 5'

AATTGCTGCAGAGACAGAGA-3', IBA-1 forward: 5'-TGAGGAGCCATGAGCCAAAG-3', IBA1 reverse: 5'- GCTT CAAGTTTGGACGGCAG-3'.

Statistical analysis

Data presented are quantified from at least three independent experiments. Student's t-test was employed to determine the statistical significance (*$p < 0.05$, **$p < 0.01$, ***$p < 0.001$) of experiment groups. All values are presented as mean ± standard error of the mean (s.e.m).

Ethical Statement

All animal procedures were performed in accordance with the Guidelines for Care and Use of Laboratory Animals of Indiana University and approved by IACUC at Indiana University Bloomington with # 18–002

Supplementary Material

Refer to Web version on PubMed Central for supplementary material.

Acknowledgment

This project was supported by the departmental start-up funds of Indiana University Bloomington, the National Science Foundation grant (CCF-1909509), and NIH awards (RF1AG056296, R01AG054102, R01AG053500, R01AG053242, R21AG050804, and 1R03EB030331). The authors thank the Indiana University Imaging Center (NIH1S10OD024988–01) and Nanoscale Characterization Facility for use of their instruments.

References

1. Gitler AD, Dhillon P and Shorter J, Dis Model Mech, 2017, 10, 499–502. [PubMed: 28468935]
2. Huang Y and Mucke L, Cell, 2012, 148, 1204–1222. [PubMed: 22424230]
3. Stephenson J, Nutma E, van der Valk P and Amor S, Immunology, 2018, 154, 204–219. [PubMed: 29513402]
4. DiSabato DJ, Quan N and Godbout JP, J Neurochem, 2016, 139 Suppl 2, 136–153. [PubMed: 26990767]
5. Lampron A, Elali A and Rivest S, Neuron, 2013, 78, 214–232. [PubMed: 23622060]
6. Eriksen JL, Acta Neuropathol, 2010, 119, 107–109. [PubMed: 20012633]
7. Stevens B, Allen NJ, Vazquez LE, Howell GR, Christopherson KS, Nouri N, Micheva KD, Mehalow AK, Huberman AD, Stafford B, Sher A, Litke Alan M., Lambris JD, Smith SJ, John SWM and Barres BA, Cell, 2007, 131, 1164–1178. [PubMed: 18083105]
8. Schafer Dorothy P., Lehrman Emily K., Kautzman Amanda G., Koyama R, Mardinly Alan R., Yamasaki R, Ransohoff Richard M., Greenberg Michael E., Barres Ben A. and Stevens B, Neuron, 2012, 74, 691–705. [PubMed: 22632727]
9. Kettenmann H, Kirchhoff F and Verkhratsky A, Neuron, 2013, 77, 10–18. [PubMed: 23312512]
10. Weinhard L, di Bartolomei G, Bolasco G, Machado P, Schieber NL, Neniskyte U, Exiga M, Vadisiute A, Raggioli A, Schertel A, Schwab Y and Gross CT, Nature Communications, 2018, 9, 1228.
11. Hemonnot AL, Hua J, Ulmann L and Hirbec H, Front Aging Neurosci, 2019, 11, 233. [PubMed: 31543810]
12. Hansen DV, Hanson JE and Sheng M, J Cell Biol, 2018, 217, 459–472. [PubMed: 29196460]
13. LaFerla FM and Green KN, Cold Spring Harb Perspect Med, 2012, 2, a006320. [PubMed: 23002015]

14. Eriksen JL and Janus CG, Behav Genet, 2007, 37, 79–100. [PubMed: 17072762]
15. Pósfai B, Cserép C, Orsolits B and Dénes Á, Neuroscience, 2019, 405, 103–117. [PubMed: 29753862]
16. Arber C, Lovejoy C and Wray S, Alzheimers Res Ther, 2017, 9, 42. [PubMed: 28610595]
17. Watson PMD, Kavanagh E, Allenby G and Vassey M, SLAS DISCOVERY: Advancing the Science of Drug Discovery, 2017, 22, 583–601.
18. Bohlen CJ, Bennett FC, Tucker AF, Collins HY, Mulinyawe SB and Barres BA, Neuron, 2017, 94, 759–773 e758. [PubMed: 28521131]
19. Cho H, Hashimoto T, Wong E, Hori Y, Wood LB, Zhao L, Haigis KM, Hyman BT and Irimia D, Scientific Reports, 2013, 3, 1823. [PubMed: 23665843]
20. Amadio S, De Ninno A, Montilli C, Businaro L, Gerardino A and Volonté C, BMC Neuroscience, 2013, 14, 121. [PubMed: 24119251]
21. Achyuta AKH, Conway AJ, Crouse RB, Bannister EC, Lee RN, Katnik CP, Behensky AA, Cuevas J and Sundaram SS, Lab on a Chip, 2013, 13, 542–553. [PubMed: 23108480]
22. Hosmane S, Tegenge MA, Rajbhandari L, Uapinyoying P, Ganesh Kumar N, Thakor N and Venkatesan A, J Neurosci, 2012, 32, 7745–7757. [PubMed: 22649252]
23. Park J, Wetzel I, Marriott I, Dreau D, D'Avanzo C, Kim DY, Tanzi RE and Cho H, Nat Neurosci, 2018, 21, 941–951. [PubMed: 29950669]
24. Pöttler M, Zierler S and Kerschbaum HH, Neuroscience Letters, 2006, 410, 137–140. [PubMed: 17084531]
25. Haw RTY, Tong CK, Yew A, Lee HC, Phillips JB and Vidyadaran S, J Neuroinflammation, 2014, 11, 134. [PubMed: 25074682]
26. Friend J and Yeo LY, Reviews of Modern Physics, 2011, 83, 647–704.
27. Yeo LY and Friend JR, Annu Rev Fluid Mech, 2014, 46, 379–406.
28. Ding X, Li P, Lin SC, Stratton ZS, Nama N, Guo F, Slotcavage D, Mao X, Shi J, Costanzo F and Huang TJ, Lab Chip, 2013, 13, 3626–3649. [PubMed: 23900527]
29. Hu X, Zhao S, Luo Z, Zuo Y, Wang F, Zhu J, Chen L, Yang D, Zheng Y, Zheng Y, Cheng Y, Zhou F and Yang Y, Lab Chip, 2020, 20, 2228–2236. [PubMed: 32441730]
30. Ozcelik A, Rufo J, Guo F, Gu Y, Li P, Lata J and Huang TJ, Nat Methods, 2018, 15, 1021–1028. [PubMed: 30478321]
31. Olofsson K, Carannante V, Ohlin M, Frisk T, Kushiro K, Takai M, Lundqvist A, Onfelt B and Wiklund M, Lab Chip, 2018, 18, 2466–2476. [PubMed: 30033460]
32. Armstrong JPK, Maynard SA, Pence IJ, Franklin AC, Drinkwater BW and Stevens MM, Lab Chip, 2019, 19, 562–573. [PubMed: 30667009]
33. Kurashina Y, Takemura K and Friend J, Lab Chip, 2017, 17, 876–886. [PubMed: 28184386]
34. Alhasan L, Qi AS, Al-Abboodi A, Rezk A, Chan PPY, Iliescu C and Yeo LY, Acs Biomaterials Science & Engineering, 2016, 2, 1013–1022.
35. Chen K, Wu M, Guo F, Li P, Chan CY, Mao Z, Li S, Ren L, Zhang R and Huang TJ, Lab Chip, 2016, 16, 2636–2643. [PubMed: 27327102]
36. Yue W, Zheng A, Bin C, Maram M, Maria B, Xiongbin L and Feng G, Journal, 2018, 29, 504006.
37. Chen B, Wu Y, Ao Z, Cai H, Nunez A, Liu Y, Foley J, Nephew K, Lu X and Guo F, Lab Chip, 2019, 19, 1755–1763. [PubMed: 30918934]
38. Guo F, Mao Z, Chen Y, Xie Z, Lata JP, Li P, Ren L, Liu J, Yang J, Dao M, Suresh S and Huang TJ, Proc Natl Acad Sci U S A, 2016, 113, 1522–1527. [PubMed: 26811444]
39. Olofsson K, Hammarstrom B and Wiklund M, Micromachines (Basel), 2018, 9, 594.
40. Gesellchen F, Bernassau AL, Dejardin T, Cumming DR and Riehle MO, Lab Chip, 2014, 14, 2266–2275. [PubMed: 24817215]
41. Murphy MP and LeVine H 3rd, J Alzheimers Dis, 2010, 19, 311–323. [PubMed: 20061647]
42. Niikura T, Tajima H and Kita Y, Curr Neuropharmacol, 2006, 4, 139–147. [PubMed: 18615127]
43. Zhang F and Jiang L, Neuropsychiatr Dis Treat, 2015, 11, 243–256. [PubMed: 25673992]
44. von Bartheld CS, Bahney J and Herculano-Houzel S, J Comp Neurol, 2016, 524, 3865–3895. [PubMed: 27187682]

45. El Khoury J and Luster AD, Trends Pharmacol Sci, 2008, 29, 626–632. [PubMed: 18835047]
46. Ramirez AI, de Hoz R, Salobrar-Garcia E, Salazar JJ, Rojas B, Ajoy D, Lopez-Cuenca I, Rojas P, Trivino A and Ramirez JM, Front Aging Neurosci, 2017, 9, 214. [PubMed: 28729832]
47. Yoon SS and Jo SA, Biomol Ther (Seoul), 2012, 20, 245–255. [PubMed: 24130920]
48. Condello C, Yuan P, Schain A and Grutzendler J, Nat Commun, 2015, 6, 6176. [PubMed: 25630253]
49. Mandrekar-Colucci S and Landreth GE, CNS Neurol Disord Drug Targets, 2010, 9, 156–167. [PubMed: 20205644]
50. Condello C, Yuan P and Grutzendler J, Biol Psychiatry, 2018, 83, 377–387. [PubMed: 29169609]
51. Plastira I, Bernhart E, Goeritzer M, Reicher H, Kumble VB, Kogelnik N, Wintersperger A, Hammer A, Schlager S, Jandl K, Heinemann A, Kratky D, Malle E and Sattler W, J Neuroinflammation, 2016, 13, 205. [PubMed: 27565558]
52. Bussi C, Peralta Ramos JM, Arroyo DS, Gaviglio EA, Gallea JI, Wang JM, Celej MS and Iribarren P, Sci Rep, 2017, 7, 43153. [PubMed: 28256519]
53. Nomura K, Vilalta A, Allendorf DH, Hornik TC and Brown GC, J Immunol, 2017, 198, 4792–4801. [PubMed: 28500071]
54. Gertig U and Hanisch UK, Front Cell Neurosci, 2014, 8, 101. [PubMed: 24744702]
55. Sochocka M, Diniz BS and Leszek J, Mol Neurobiol, 2017, 54, 8071–8089. [PubMed: 27889895]
56. Wang WY, Tan MS, Yu JT and Tan L, Ann Transl Med, 2015, 3, 136. [PubMed: 26207229]
57. Hopperton KE, Mohammad D, Trepanier MO, Giuliano V and Bazinet RP, Mol Psychiatry, 2018, 23, 177–198. [PubMed: 29230021]
58. Li B, Yamamori H, Tatebayashi Y, Shafit-Zagardo B, Tanimukai H, Chen S, Iqbal K and Grundke-Iqbal I, J Neuropathol Exp Neurol, 2008, 67, 78–84. [PubMed: 18091557]

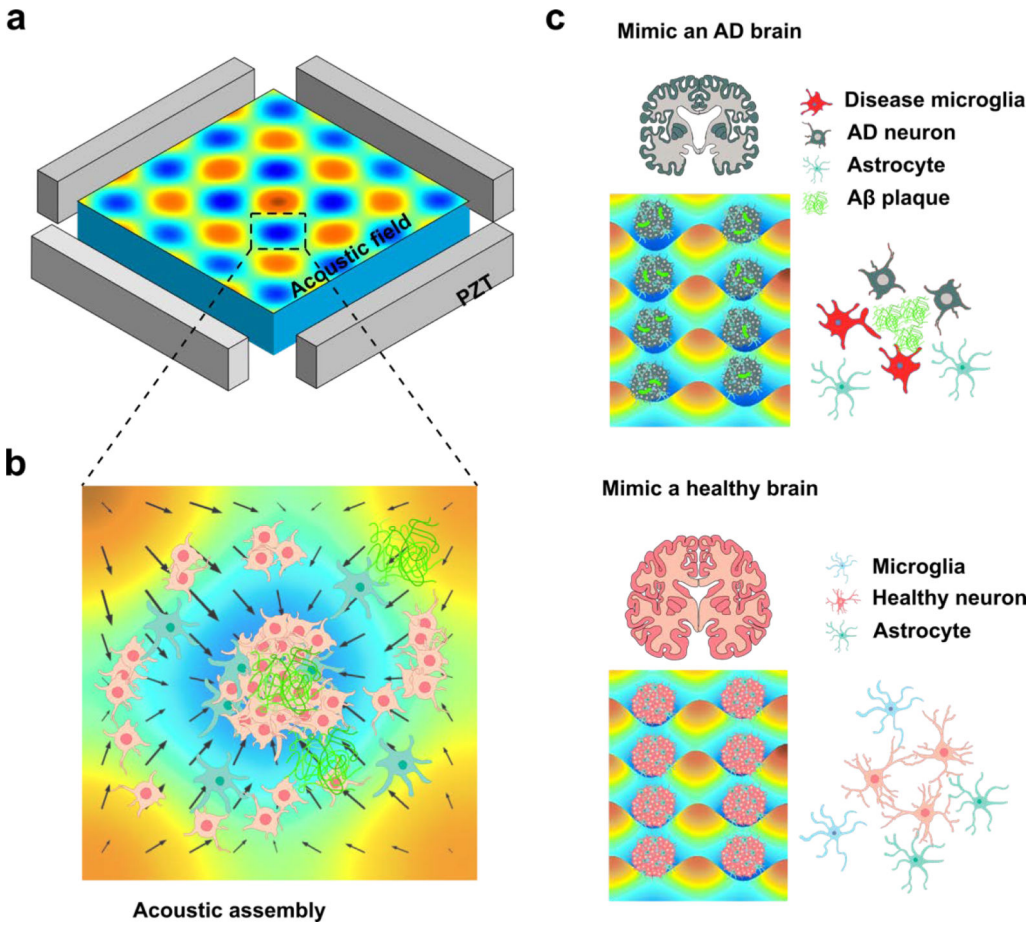

Figure 1. Acoustofluidic assembly of 3D neurospheroids to model Alzheimer's disease.

(a) Schematic of the acoustic assembly device. The rainbow color maps the numerical simulation results of the acoustic Gor'kov potential field in the acoustic assembly chamber. Red and blue colors indicate anti-pressure and pressure nodes, respectively. (b) The acoustic assembly process of 3D neurospheroids. (c) Schematics of the acoustically-assembled 3D neuronal cultures to model AD. The 3D neurospheroids were generated via acoustic assembly with uniform size. By controlling the cellular and environmental components, the acoustically-assembled 3D neurospheroids can mimic the cell interaction and their microenvironment in normal and AD brain.

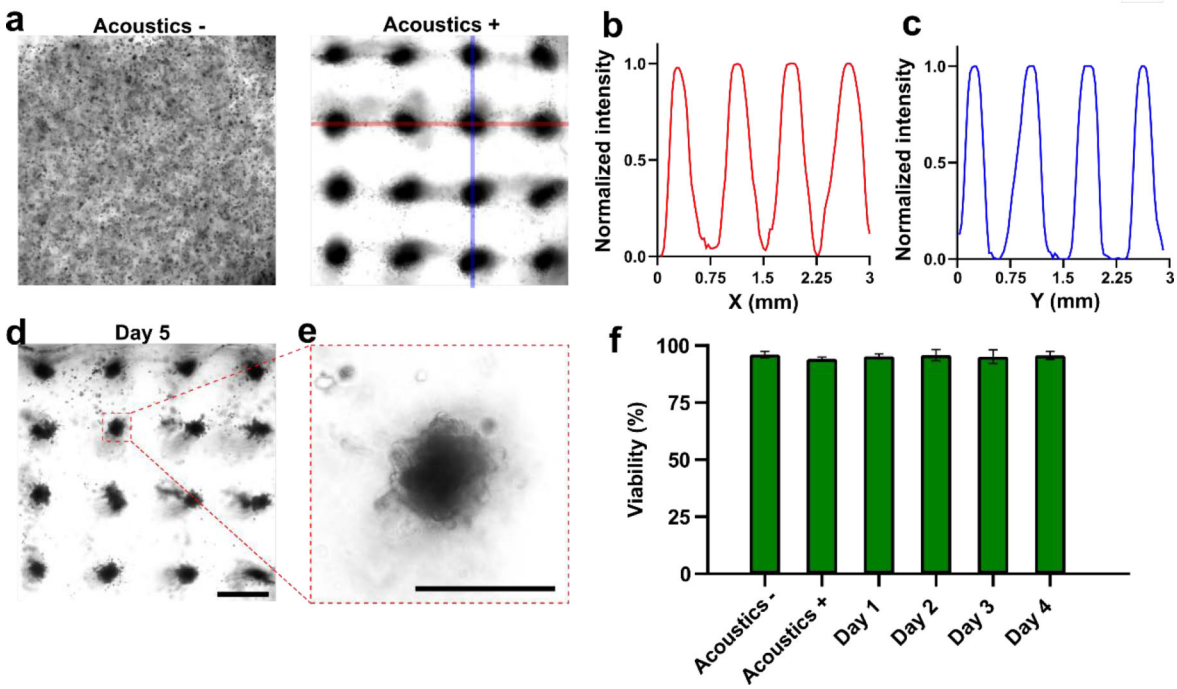

Figure 2. Acoustic cell clustering.

(a) The acoustic assembly process of N2A cell clusters. When applied with acoustic waves, randomly distributed cells (“Acoustics −”) migrate and form arbitrary patterned cell clusters (“Acoustics +”). (b, c) The measured brightness of pattern image along the X and Y-axis corresponding to the red and blue area in (a). The brightness result was normalized to the maximum brightness of the image. (d) Acoustic patterned N2A cell clusters after a 5-day culture. Assembled N2A cells aggregated together and formed firm neurospheroids. (e) Detailed view of single acoustic assembled N2A cell cluster after 5-day culture. (f) The cell viability was measured by LIVE/DEAD™ kit, before and right after acoustic assembly, and during cell culture after the acoustic assembly. Data represent means ± s.e.m. (Scale bar = 500 μm)

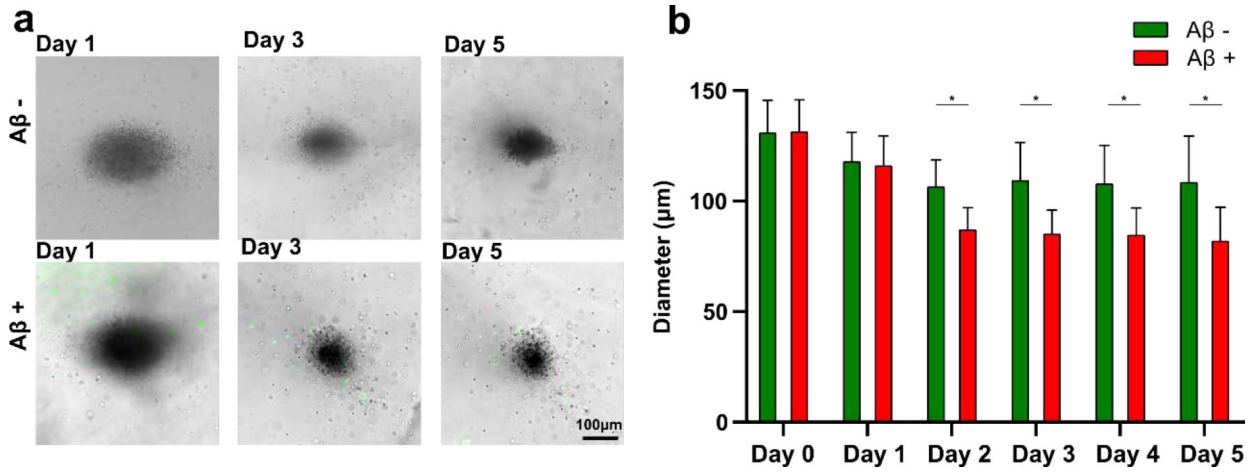

Figure 3. Amyloid-β Neurotoxicity tests in 3D neurospheroids.

(a) Time-lapse images of primary 3D neurospheroids with or without Aβ aggregates from day 1 to day 5. The Aβ aggregates were labeled with a green fluorescent antibody against Aβ. (b) The size distribution of 3D neurospheroids with or without Aβ aggregates over time. Data represent means ± s.e.m. of 3 independent experiments (n=20, $*p < 0.01$). (Scale bar = 100)

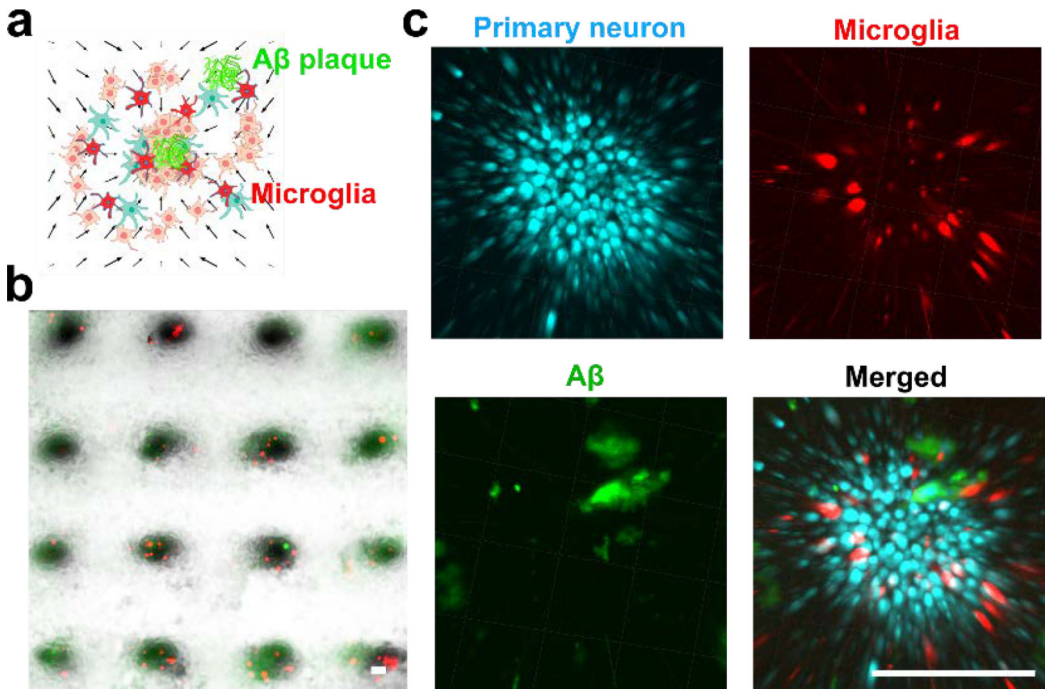

Figure 4. Modeling Alzheimer's Disease.

(a) Schematic of acoustically assembled 3D culture model of AD. Primary neurons (Blue), microglia (Red), and Aβ aggregates (Green) were acoustically assembled into 3D neurospheroids patterns. (b) The acoustically assembled 3D neurospheroids of AD. (c) Separate 3D reconstructed confocal images of the primary neuron (Blue) stained with CFSE dye, microglia (Red) labeled with CMTPX dye, Aβ aggregates (Green) stained with anti-Aβ 6E10 antibody, and merged images of these three colors. Microglia (Red) and Aβ aggregates (Green) were randomly distributed in the acoustically-assembled primary 3D neurospheroids (Blue). (Scale bar = 200 μm)

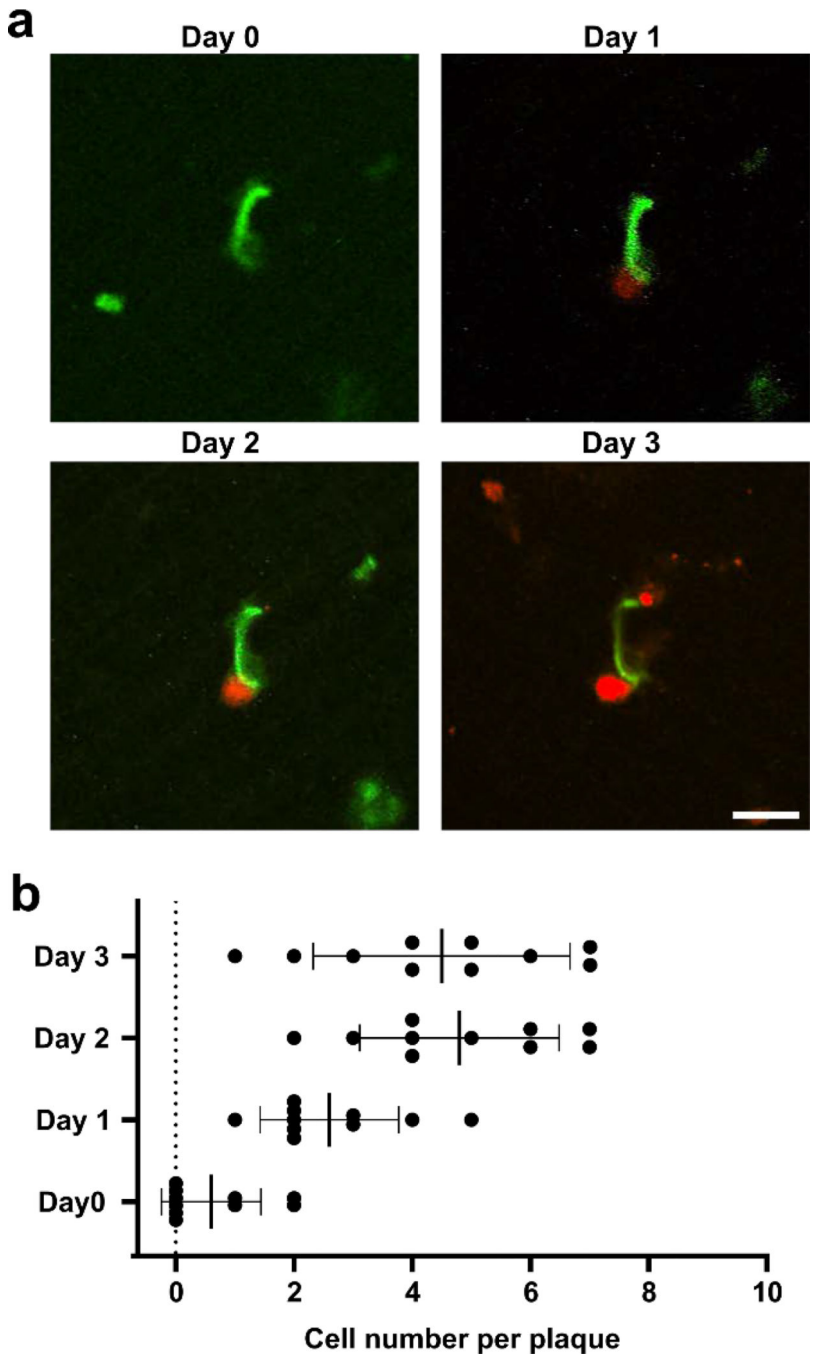

Figure 5. Accumulation of microglia around Amyloid-β aggregates within a 3D neurospheroid.

(a) Representative confocal time-lapse images of a red fluorescent dye (CMTPX)-labeled microglia (BV-2) around Aβ aggregates (green) stained with anti-Aβ 6E10 antibody in an acoustically assembled neurospheroid. (b) Quantification of microglia accumulation around Aβ aggregates over time. Microglia accumulation was quantified as the microglial cell numbers within 20 μm distance from Aβ aggregates. N > 10 aggregates (1 – 40 μm in diameter) from different acoustic assembled 3D neurospheroids. Bars represent mean ± s.e.m. (Scale bar = 20 μm)

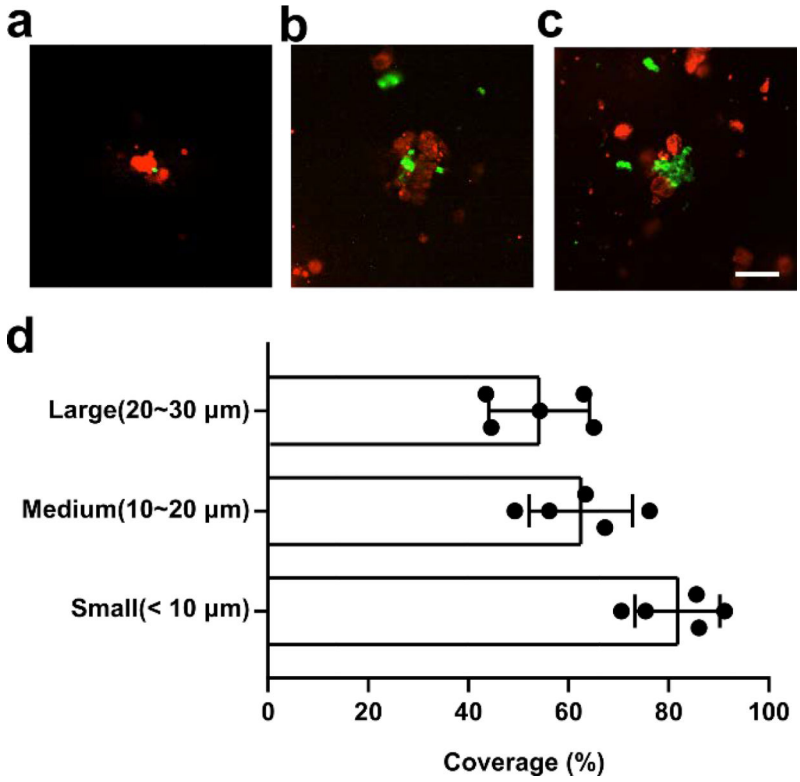

Figure 6. Coverage of microglia to Amyloid-β aggregates within a 3D neurospheroid.

Representative confocal time-lapse images of small (a), medium (b), and large (c) sized Aβ aggregates (green) stained with anti-Aβ 6E10 antibody covered by microglia (stained by CMTPX dye in red) in an acoustically assembled neuronal spheroid. (d) Quantification of microglia coverage in an acoustically assembled 3D neurospheroids. Microglia coverage was quantified as the percentage of aggregate perimeter contacted by the microglia process. Black bars represent mean ± s.e.m. (Scale bar = 20 μm)

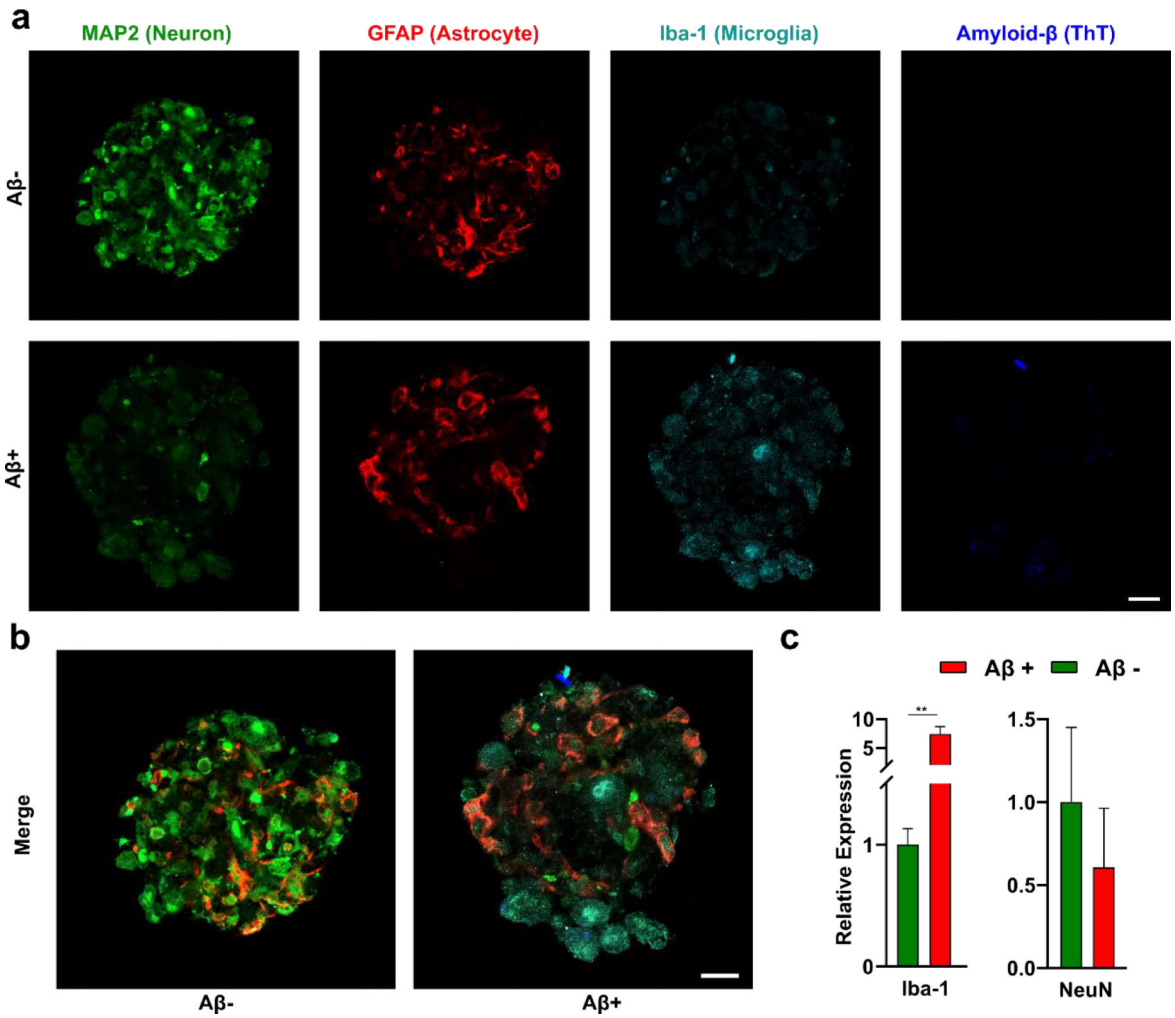

Figure 7. Microglia activation in 3D neurospheroids.

(a) Representative confocal images of immune-stained acoustically-assembled 3D neurospheroids after a 5-day culture without (top panel) or with (bottom panel) Aβ aggregates. (b) Merged fluorescence confocal images of neurospheroids without or with Aβ aggregates. (c) qRT-PCR results of Iba-1 and NeuN expression in acoustically assembled 3D neurospheroids after a 5-day culture without or with Aβ aggregates. Black bars represent mean ± s.e.m. (Scale bar = 20 μm)